An Analysis of Pack Ice Drift in Summer

MILES G. MCPHEE

ABSTRACT

Periods of *free drift*, when the internal stress divergence in pack ice is minimal, are identified during the melt season of 1975 by considering inertial oscillations, ice-wind-current statistics, and direct simulations of ice drift at the AIDJEX stations. Working from a simple balance of wind stress, water drag, and Coriolis force, it is shown that the water stress magnitude is well described by the relationship $|\tau_w| = c_w |\mathbf{V}|^2$, where $\mathbf{V}$ is the ice velocity relative to the ocean; that the oceanic boundary-layer turning angle is probably in the range $21° < \beta < 26°$; and that the ratio c_w/c_{10}, where c_{10} is the 10 m wind drag coefficient, is about 2. Times are also shown when simulations of velocity gradients using a uniform free-drift model across the manned ice station array agree reasonably well with observations. Similar calculations with geostrophic winds show many of the same features, but are not as close quantitatively.

INTRODUCTION

An important question for any dynamical modeling of pack ice is the extent to which variations in the "external" driving forces—i.e., air stress, water drag, or mean ice thickness—are separable from variations caused by mechanical forces within the pack. A. Thorndike (personal communication, 1976) has shown that, given measured ice velocity and reasonable ranges for the external parameters, one can construct limits for the wind velocities which would allow a simple balance of external forces. Unless the observed wind falls convincingly outside these limits, the ice motion is indiscernible from a state of free (or wind-driven) drift in which internal ice forces are negligible. Unfortunately, there are large uncertainties in our understanding of both boundary layers, and to a lesser extent the mean ice thickness; thus, the test is restrictive in the sense that it classifies as

free drift many periods during which we feel intuitively that internal ice stress must play an important role.

A different approach is this: rather than look for large internal forces, we try instead to identify "control" cases for which we are relatively confident that internal stress gradients are small. We may then use wind and drift data to tie the external parameters together with much greater precision than if they were all considered separately. Using other data to extrapolate any changes that might occur in the external parameters over time, we are thus provided with a much less encompassing definition of free drift. In this paper, we begin such a study using data from the AIDJEX camps taken in the summer of 1975.

FREE DRIFT

What evidence suggests that internal ice stress is not an important factor in summertime ice dynamics? It seems obvious that the fragmented summer pack should not be able to support as much internal stress as the winter pack, but does this necessarily mean that floe interactions are negligible in the total momentum balance? In this section we pursue three somewhat independent lines of reasoning which all indicate that for several weeks during the melt season of 1975 the ice was effectively free of internal forces.

Inertial Oscillations

One of the most striking differences between ice drift during summer and the remainder of the year is the presence of large-amplitude inertial motions. Hunkins (1967), using data from deep current meters, identified cycloidal loops having inertial periods in the drift of T-3 and he related them qualitatively to changes in the local wind stress. With fixed current meters and highly accurate navigation at the manned AIDJEX stations, we were able to monitor similar motions closely. By solving a simple time-dependent momentum equation that includes the inertia of the water column, we can simulate the velocity waves with fair success (McPhee, 1977), an indication that they are generated by local winds.

Figure 1 shows the zonal component of ice velocity at station Caribou measured with respect to three references. The top trace is the absolute velocity from smoothed NavSat data; the second trace is the velocity with respect to a level 30 m below the ice taken from hourly averages of a current meter suspended there; and the bottom trace is a similar determination of the velocity relative to a current meter at 2 m. Although the NavSat processing attenuates some of the energy at the inertial period, particularly if the satellite fix rate falls off (Thorndike and Cheung, 1977), the short period definition is good enough to indicate that there is not much *absolute* current at 30 m. On the other hand, the lack of relative inertial motion between the ice and 2 m implies a large inertial component at that level, and thus that the upper ocean oscillates with the ice.

During the remainder of the experiment (i.e., prior to day 181 and after day

281), the inertial component was small, even though the ice was often relatively mobile. (We use the AIDJEX convention of expressing time in days beginning with 1 January 1975; 1 January 1976 is day 366.)

Our experience at camp Jumpsuit in March and April 1972 was similar: the ice appeared to move quite freely in response to surface winds, but inertial motion was damped so rapidly as to be barely perceptible. A plausible explanation is that the scale over which the inertial motions are coherent is considerably less than the scale of the major atmospheric disturbances causing the mean motion, so that even though a whole region of ice is moving with little apparent resistance, differential motion on smaller scales is rapidly quelled by internal stresses. In the summer, this smaller-scale resistance is much reduced, and the boundary layer of the ocean, including the floes, behaves more like that of the open sea. If the ice cannot transmit force on these scales, it is difficult to see how it could over larger areas.

The fact that inertial motion is so pronounced during the summer also influences our definition of water stress. We have shown (McPhee, 1977) that for time scales short compared with the inertial period it is not appropriate to think of the ocean as exerting a passive drag on the ice because the water column possesses a large fraction of the total momentum of the system. Simulations have indicated, however, that the nonlinear effects of the waves are not large; i.e., the output of the inertial model, when filtered, is not much different from a passive-drag simulation. In what follows, therefore, the ice velocity, current, and wind

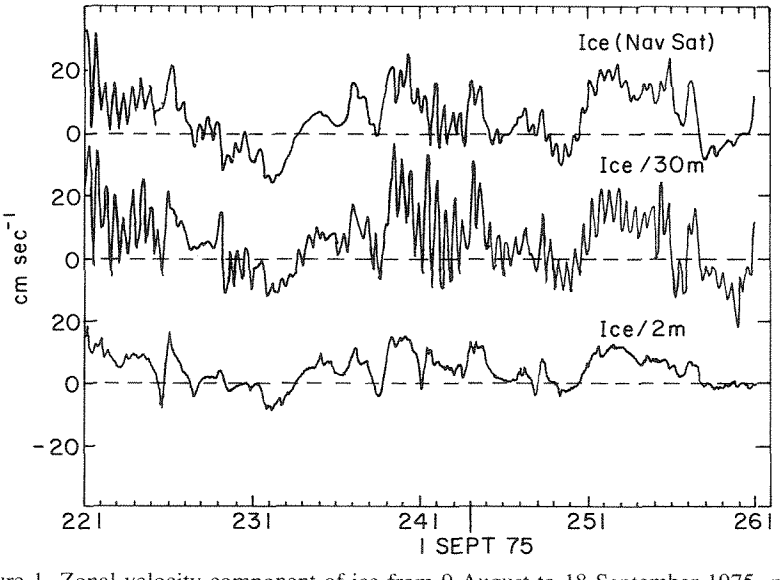

Figure 1. Zonal velocity component of ice from 9 August to 18 September 1975, measured by navigation (top); with respect to the 30 m level in ocean (middle); with respect to the 2 m level in ocean (bottom).

records have been filtered with a 12-hour cosine-bell convolution to remove most of the inertial energy, unless otherwise noted.

Wind-Ice-Current Statistics

Another approach to identifying free-drift conditions is to consider the relationship between ice drift and surface wind, e.g., the ratio of ice speed to wind speed (the well-known 2% rule). Before doing that, it is useful to discuss the free-drift momentum balance.

For convenience we describe the force balance sketched in Figure 2 using complex notation for horizontal vectors, so that an arbitrary vector $\mathbf{A} = A_x\ \mathbf{e}_x + A_y\ \mathbf{e}_y$ is identical to $\mathbf{A} = Ae^{i\gamma}$, where $\gamma = \arctan(A_y/A_x)$ and A is the scalar magnitude. Thus, for steady drift with no internal ice force, the balance is

$$\rho_a c_{10} U_{10} \mathbf{U}_{10} = imf\mathbf{V} - \rho_w \tau_w \tag{1}$$

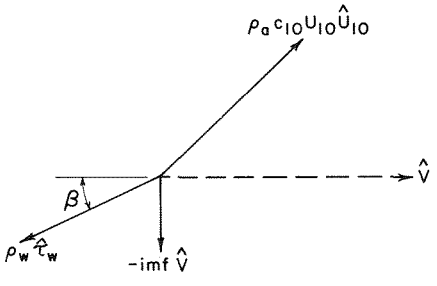

Figure 2. Schematic of the free-drift force balance.

where ρ_a and ρ_w are air and water densities; c_{10} is the drag coefficient appropriate for the surface wind, $\mathbf{U}_{10}$; f is the Coriolis parameter; m is the ice mass per unit area, τ_w is the kinematic water stress; and $\mathbf{V}$ is the ice velocity relative to the undisturbed ocean current $\mathbf{V}_g$ (the effect of sea-surface tilt is thus implicit in $\mathbf{V}$, since the ice force due to tilt is $-imf\mathbf{V}_g$).

In the AIDJEX ice model water stress is related to $\mathbf{V}$ (McPhee, 1975) by

$$\tau_w = -c_w\ V\ \mathbf{V}\ e^{i\beta}$$

where c_w and β are experimentally determined boundary-layer parameters. Let δ be the angle from ice drift to surface wind direction. Then rearrangement of the momentum equation (1) yields

$$\frac{U_{10}^2}{V^2} e^{i\delta} = \frac{\rho_w c_w}{\rho_a c_{10}} \left\{ e^{i\beta} + \frac{mf}{\rho_w c_w V} e^{i\pi/2} \right\}$$

Note that if the ice mass were small enough to make the Coriolis term negligible, a very simple expression would result, with $\delta = \beta$ and the speed ratio constant.

However, with realistic estimates of the physical quantities—m $\sim$ 300 gm cm^{-2}, $f \sim 1.4 \times 10^{-4}$ sec^{-1}, $c_w \sim 5 \times 10^{-3}$—then for $V \sim 20$ cm sec^{-1}, the ratio, $mf/\rho_w c_w V$ is about 0.5. Thus, the second term on the right-hand side of (2) is clearly important, and for this reason we expect δ to be greater than β. (As an aside, it appears that ice modelers are alone in appreciating that the *Fram* drifted 45° to the right of the wind more because of the mean thickness of pack ice than because of constant eddy viscosity in the Ekman layer.)

With these preliminaries out of the way we return to the question of ice drift-wind ratios, which are shown in Table 1. To arrive at these values, we sampled smoothed records of ice and wind velocity twice daily at each of the four manned camps: Big Bear (BB), Caribou (CA), Blue Fox (BF), and Snow Bird (SB). The resulting complex ratios were averaged in 20-day blocks using all samples for which the wind speed was greater than 2.5 m sec^{-1}. Results are shown as the magnitude of the ratio in percent and the angle of rightward deflection (δ) in degrees. Note that both quantities reach maxima during the summer (days 181 to 261) and that the variance from camp to camp is markedly less then.

Although perhaps not obvious *a priori*, the fact that during winter δ is usually smaller than the free-drift value probably reflects the fact that, in a mean sense, the center of the Beaufort Gyre is a region of convergence and thus the average stress gradient will act toward the left of the wind, decreasing the deflection angle. The same effect is apparent in observations that the ice tends to follow atmospheric isobars.

The ratios shown in Table 1 are not particularly significant for determining drag parameters since, as we have shown above, the Coriolis force causes the ratio to be a nonlinear function of V. It is a fairly simple matter, however, to extend this type of analysis to determination of the water stress as long as we can assume free drift. With this in mind we chose the 20-day period at the height of the melt season, days 221–241 (9–29 August 1975), for which the drift ratio was consistently high, and performed regression analysis of water stress magnitude against ice speed. The water stress was calculated from the force balance shown in Figure 2 using the measured 10 m wind, the measured ice velocity, and realistic estimates for c_{10}, m, and $\mathbf{V}_g$.

The 10 m drag coefficient used here is 0.0027 (E. Leavitt, personal communication). The mean ice mass, m, was taken to be 300 gm cm^{-2} on the basis of thickness surveys at Big Bear (A. Hansen, personal communication). Geostrophic flow, $\mathbf{V}_g$, is taken from a dynamic topography compiled by Newton (1973). It is by no means certain that a historical topography is appropriate, particularly during 1975, when ice drift patterns were anomalous, but at this time it represents our best estimate. Flow in the vicinity of the camps was thought to be on the order of 2.5–3.0 cm sec^{-1} toward the west, although there are some indications that these magnitudes are high.

The water stress, τ_w, was calculated from the force balance (1) for two samples from each camp each day during the 20-day period. Those samples for which the relative ice speed $V = |\mathbf{V}_i - \mathbf{V}_g|$ was less than 8 cm sec^{-1} were

TABLE 1

RATIO OF ICE VELOCITY TO WIND VELOCITY

Period	Ice/Wind (%)					Angle of Rightward Deflection (deg)					No. of Samples			
(AIDJEX Days)	BB	CA	BF	SB	Avg.	BB	CA	BF	SB	Avg.	BB	CA	BF	SB
101–121	0.90	1.35	1.98	1.22	1.11	66.7	42.1	36.2	46.5	56.9	24	4	3	11
121–141	1.63	1.59	1.37	1.60	1.54	34.6	25.9	33.6	32.3	31.7	31	29	35	24
141–161	1.53	1.56	1.60	1.61	1.58	43.5	36.8	36.4	34.8	37.7	29	32	36	30
161–181	1.65	1.61	1.49	1.60	1.59	44.6	39.6	41.6	46.8	43.2	28	30	28	33
181–201	1.92	1.87	1.96	2.00	1.94	44.3	44.5	47.9	48.6	46.3	33	33	32	31
201–221	1.96	1.77	2.02	2.02	1.93	45.9	48.9	47.7	43.8	46.5	38	38	25	37
221–241	2.13	1.96	2.15	2.18	2.10	48.2	46.4	50.6	47.6	48.2	34	35	34	33
241–261	1.86	1.87	1.93	1.98	1.91	46.6	45.1	50.8	44.9	46.0	37	36	35	37
261–281	...	1.82	1.85	1.84	1.84	...	39.6	43.9	36.5	40.2	0	29	36	32
281–301	...	1.53	1.53	1.57	1.54	...	39.4	46.1	35.8	40.7	0	35	35	29
301–321	...	1.06	1.09	0.92	1.02	...	31.9	36.6	32.1	33.2	0	32	20	23
321–341	...	1.15	0.99	1.18	1.11	...	29.2	37.1	27.3	31.0	0	32	28	32
341–361	...	0.95	0.76	0.80	0.84	...	32.9	33.3	20.1	29.0	0	32	34	30
361–381	...	1.13	1.04	1.02	1.07	...	36.4	44.0	29.9	36.8	0	36	35	34
381–401	...	0.75	0.57	0.82	0.71	...	21.8	29.9	25.2	25.8	0	32	36	30
401–421	...	0.29	0.20	0.29	0.26	...	22.4	13.9	27.8	21.3	0	32	37	37
421–441	...	1.07	0.48	1.01	0.81	...	30.5	23.6	13.8	24.0	0	29	32	17
441–461	...	0.13	0.04	0.22	0.13	...	33.5	32.5	24.3	30.3	0	31	34	29
461–481	...	0.76	0.58	0.82	0.71	...	21.3	22.2	21.5	21.7	0	31	30	23
Average	1.74	1.28	1.20	1.33	1.33	46.3	35.2	37.2	34.2	36.9	254	588	585	552

NOTE: Integers on right indicate number of samples in each 20-day average.

rejected because of uncertainty in $\mathbf{V}_g$, leaving 95 points which are plotted as a scatter diagram in Figure 3. A least-squares straight line fit through the origin with slope $c_L = 0.086$ is shown with dashes. The other dashed curve is a least-squares fit parabola through the origin with $c_w = 0.0055$. Finally, the solid curve is a least-squares fit exponential of the form

$$\tau_w = aV^b$$

where $b = 2.05$ with a 90% confidence interval of 1.86–2.25. The value for the exponent is not affected much by variation in ice mass or c_{10}; e.g., with $m = 250$ gm cm^{-2} and $c_{10} = 0.002$, the confidence interval was identical.

This result has two rather important implications. First, the quadratic dependence for the water stress appears justified. Linear water stress, which the classical Ekman approach predicts, is attractive in that it simplifies model calculations; but neither our measurements in the oceanic boundary layer (McPhee and Smith, 1976) nor these results support it. Second, the water drag coefficient is about twice the air coefficient over a reasonable range of c_{10} ($c_w = 0.0055$ for $c_{10} = 0.0027$, $c_w = 0.0040$ for $c_{10} = 0.002$). Because of the wide range of c_{10} reported in the literature, maintaining this ratio is probably more appropriate than specifying a particular value for c_w.

Theoretically, the above calculation should also furnish the oceanic boundary-layer angle, β. In practice, β calculated this way is sensitive to assumptions about m, c_{10}, and $\mathbf{V}_g$. The mean value found using the above parameters was about 19°, but other evidence indicates that this is somewhat low. Table 2 is similar in format and preparation to Table 1, except that the complex ratios of the 2 m relative current over the negative ice velocity have been averaged using

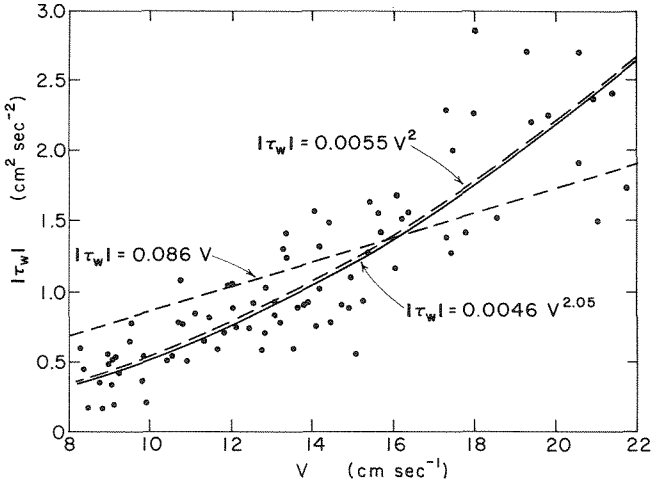

Figure 3. Kinematic water stress versus relative ice speed.

TABLE 2

RATIO OF 2 m RELATIVE CURRENT TO NEGATIVE ICE VELOCITY

	Current Ice					Ocean Boundary Layer Angle (deg)					No. of Samples			
Period	BB	CA	BF	SB	Avg.	BB	CA	BF	SB	Avg.	BB	CA	BF	SB
101–121	0.54	...	...	...	0.54	16.6	...	...	...	16.6	1	0	0	0
121–141	0.66	0.63	...	...	0.65	15.9	16.6	...	...	16.2	4	3	0	0
141–161	0.67	...	...	...	0.67	14.9	...	...	...	14.9	1	0	0	0
161–181	0.61	0.72	0.67	...	0.68	24.4	14.6	31.7	...	23.4	1	2	2	0
181–201	0.63	0.67	0.69	...	0.66	23.5	18.6	23.9	...	22.0	13	14	15	0
201–221	0.57	0.61	0.61	0.61	0.60	20.7	33.0	8.9	23.6	20.8	11	9	11	8
221–241	0.62	0.58	0.58	0.56	0.59	26.5	34.2	22.5	18.9	25.2	14	12	12	15
241–261	0.62	0.58	0.60	0.63	0.61	27.2	36.0	23.7	23.1	27.2	11	9	8	13
261–281	...	0.58	0.54	0.59	0.57	...	28.1	17.4	26.4	24.6	0	10	6	5
281–301	...	0.58	0.63	0.50	0.59	...	21.6	22.8	29.2	23.6	0	3	6	2
301–321	...	0.63	0.53	0.53	0.56	...	30.5	22.1	23.7	25.7	0	6	4	7
321–341	...	0.61	0.53	0.62	0.60	...	21.0	17.5	21.4	20.5	0	7	3	6
341–361	...	0.64	0.64	0.58	0.62	...	25.6	37.2	23.5	30.9	0	1	2	1
361–381	...	0.66	0.63	0.66	0.65	...	23.4	28.1	25.7	25.3	0	8	5	3
381–401	...	0.64	0.76	0.64	0.69	...	12.6	26.3	17.4	19.9	0	2	3	2
401–421	...	0.58	...	0.77	0.71	...	22.5	...	19.9	20.8	0	1	0	2
421–441	...	...	0.82	...	0.82	...	...	4.6	...	4.6	0	0	1	0
441–461	...	...	...	...	...	...	...	...	...	...	0	0	0	0
461–481	...	...	...	...	...	...	...	...	...	...	0	0	0	0
Average	0.62	0.62	0.62	0.60	0.61	23.6	26.5	21.3	22.4	23.6	56	87	78	64

smoothed samples for which the current speed was greater than 8 cm sec^{-1}. Since the relative current near the surface is in the direction of water stress, the angular part of the ratio is a good approximation to β. Unlike its ice/wind counterpart, this ratio is not dependent on internal ice stress, but is instead a boundary-layer parameter expected to remain relatively constant from Rossby-number similarity theory (McPhee, 1975). Maintaining alignment of current meters to within a couple of degrees is difficult, and individual samples and even 20-day averages are undoubtedly affected by $\mathbf{V}_g$. Considering these and other sources of error, the uniformity of the yearly averages for β is surprising.

Boundary-layer measurements made during a storm at the 1972 pilot study camp Jumpsuit (McPhee and Smith, 1976) suggested a mean value of 24° for β, but the ratio U_2/V was closer to 0.85, thus the under-ice surface at Jumpsuit must have been considerably smoother. This may help to explain the increased drag coefficient: 0.0034 for 1972 compared with 0.0055 for 1975. That the average small-scale roughness as indicated by U_2/V was so uniform for the four camps is quite amazing.

Free-Drift Simulations

The third approach is simply to simulate ice drift assuming no internal forces and compare the results with observations. Figure 4 shows a 40-day simulation during summer. For each camp the steady-state momentum balance (1) was solved for $\mathbf{V}$ every 3 hours, then the magnitude of $\mathbf{V}$ was plotted as a solid line

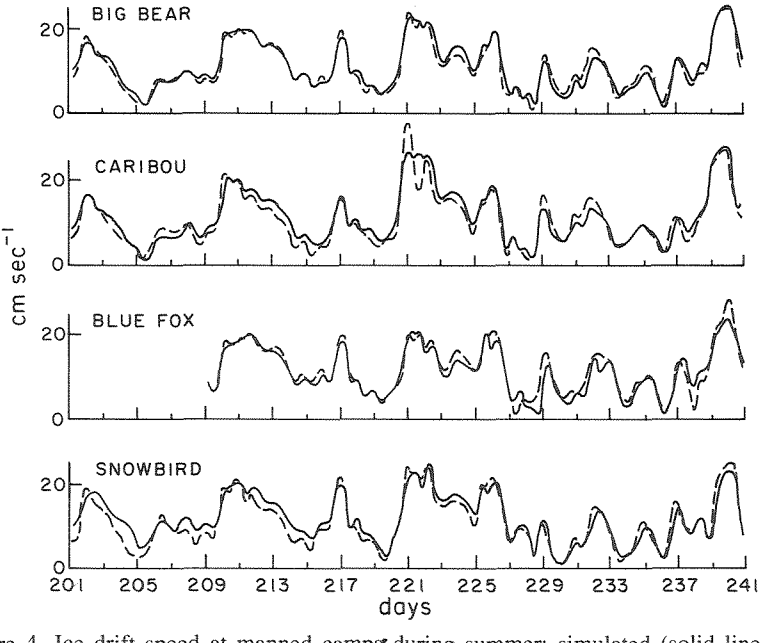

Figure 4. Ice drift speed at manned camps during summer: simulated (solid line), observed (broken line).

and the observed ice speed as a dashed line. Drag parameters were the same for all camps: $c_{10} = 0.0027$, $c_w = 0.0055$, and $\beta = 23°$. Since no account of $\mathbf{V}_g$ was taken, we expect errors of as much as 2–3 cm sec^{-1}, and the difference between simulated and observed speeds only occasionally exceeds that.

Figure 5 shows a similar exercise during the winter with the same drag coefficients. It is fairly obvious that the differences between observation and simulation cannot be eliminated by adjusting drag coefficients; e.g., compare the deceleration observed at Snow Bird starting about day 387 with the steady free-drift prediction.

On short time scales under moderate or higher winds, the effect of geostrophic ocean currents on the momentum balance and velocity gradients is probably small, especially near the center of the Beaufort Gyre where the camps were first located. On the other hand, advection by ocean currents becomes a large part of the total trajectory over longer periods; e.g., a steady 1 cm sec^{-1} current amounts to about 18 km over a 20-day period.

In looking at drift records, we noticed that during days 181–201 station Caribou drifted right across the center of the Gyre according to Newton's (1973) dynamic topography (75.7°N, 147°W), and we might expect the smallest currents there. Using the inertial free-drift model (McPhee, 1977) with relatively strong damping because the inertial waves were not as large as they were later in the season, we calculated the drift of Caribou in response to surface wind alone as shown by the solid line in Figure 6, compared with the observed trajectory (dashed). Drag parameters were the same as above, with the damping coefficient (see McPhee, 1977, p. 69) $d_0 = 2.0$.

Although this result is probably in part fortuitous, it is interesting to contemplate that one might navigate by wind for 20 days and always know one's

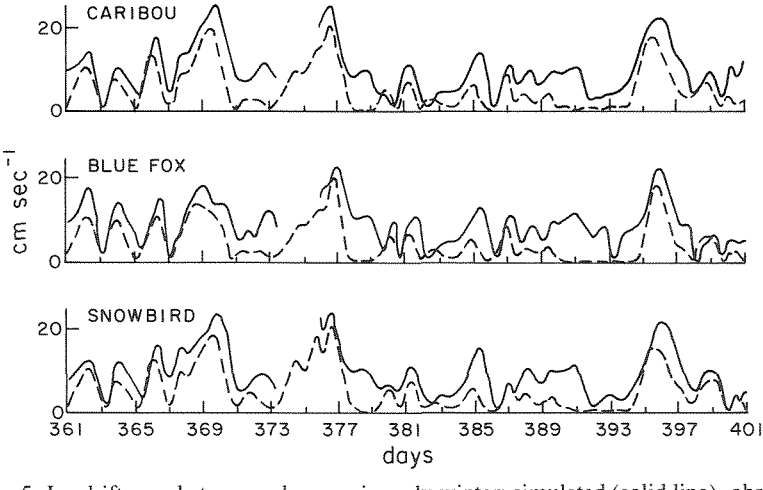

Figure 5. Ice drift speed at manned camps in early winter: simulated (solid line), observed (broken line).

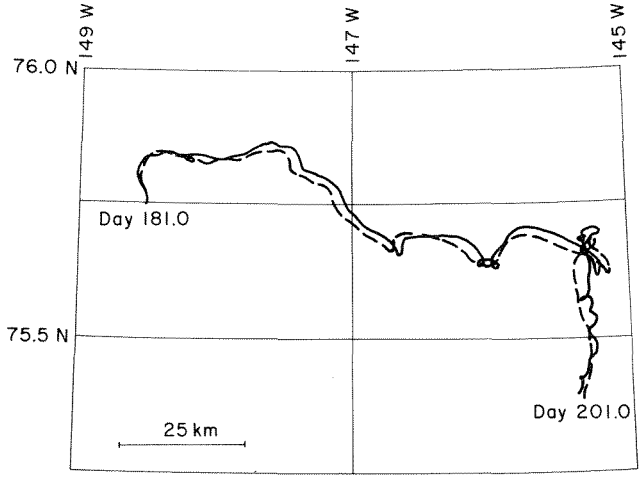

Figure 6. Drift trajectory of station Caribou days 181–201: Simulated with free-drift model including oceanic boundary layer inertia (solid line), observed (broken line).

position to within about 3 km, given the proper drag coefficients. In a more serious vein, such simulations may be useful for inferring currents from residual drift as was done by Nansen and others (e.g., Petrichenko, 1940), who assumed a simpler linear relation between wind and ice drift.

FREE-DRIFT VELOCITY GRADIENTS

A crucial question for interpreting the output of dynamic ice models is the extent to which factors outside the ice model itself affect differential motion on scales over which the ice is considered a continuum. For instance, consider an array of points freely drifting so that the velocity at each is a function of only the local wind, current, and ice thickness and roughness characteristics. How much do variables having nothing to do with the constitutive law for pack ice (like local changes in drag parameters, or variations in surface wind not apparent in the geostrophic wind) affect our ability to simulate differential motion? Borrowing heavily on drift analysis techniques advanced by R. Colony (personal communication), we approximated free-drift velocity gradients across the triangular array calculated both from measured surface winds and from geostrophic winds obtained by surface pressure analysis.

Describing each velocity component as a plane across the array, e.g., $u = Ax + By + C$, we solve for the coefficients which provide first-order estimates for the velocity gradient components ($A \doteq \partial u/\partial x$). With four camps this can be done in a least-squares sense, but because the weighting of the central main camp is small, for simplicity we fit the plane using only the outer triangle camps: Caribou, Blue Fox, and Snow Bird.

The velocity-gradient tensor may be decomposed into symmetric and antisymmetric parts, with the latter characterized by the scalar vorticity. The symmetric part is identified with the strain-rate tensor from continuum mechanics, which provides a convenient notational framework despite the fact that an ice continuum has no meaning for the free-drift state. Following conventional analysis of two-dimensional symmetric tensors, we rotate the tensor into a reference frame for which the off-diagonal elements vanish, leaving two ordered *principal strain rates*.

To compare simulated and observed gradients, the following was done. First, all time series of wind and velocity were smoothed with a 24-hour filter. Then time series of free-drift velocities were generated at each camp using (1) with the usual drag parameters: $c_{10} = 0.0027$, $m = 300$ gm cm^{-2}, $c_w = 0.0055$, and $\beta = 23°$. Next, similar series were calculated for each camp using a derived surface wind, $\mathbf{U}_s$, such that

$$\mathbf{U}_s = \sqrt{c_g/c_{10}}\, \mathbf{U}_g\, e^{i\alpha}$$

where $\mathbf{U}_g$ is the geostrophic wind, with $c_g = 0.0011$ and $\alpha = 20°$. The vorticity and strain-rate principal values were calculated for these series and the observed velocity series. Results are shown in Figures 7 and 8. For brevity, we show only the first principal value; with respect to intercomparison of the three time series, the second principal value is not much different. Although it is difficult to draw definite conclusions, it would appear on the basis of the similarity between the observed and 10 m simulations, especially for the ten days starting about day

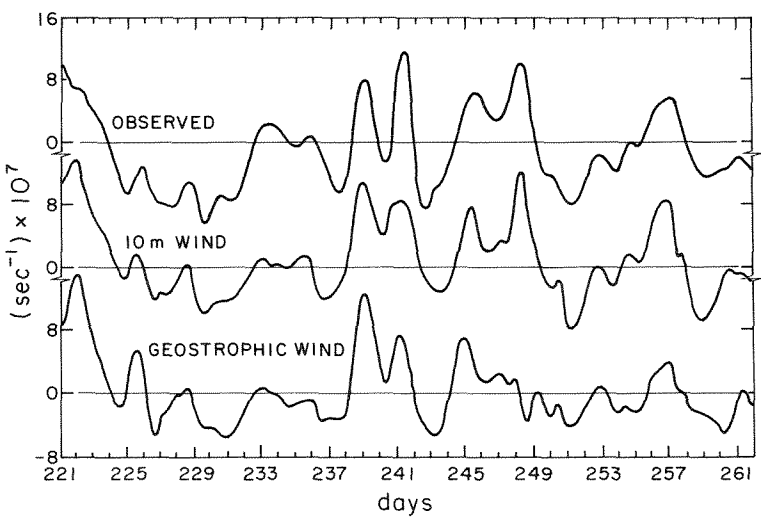

Figure 7. Vorticity of manned camp triangle: observed (top); simulated with 10 m wind (middle); simulated with geostrophic wind (bottom).

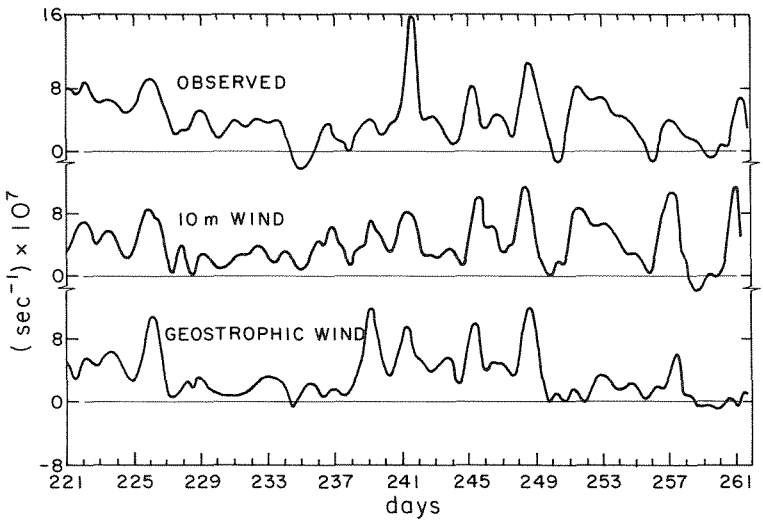

Figure 8. First principal value of strain rate: observed (top); simulated with 10 m wind (middle); simulated with geostrophic wind (bottom).

245, that variation of drag parameters is not a major cause of velocity differentials.

During the same period the geostrophic winds do a relatively poorer job. More work is required for a quantitative measure of how well the geostrophic wind produces the same effect as the observed surface wind, but these plots provide a qualitative feel.

It should be noted in passing that the divergence of the strain-rate tensor (a useful quantity for estimating open water, etc.) is the sum of the two principal values. Since they are often of comparable magnitude but opposite sign, the errors apparent in Figure 8 are relatively more important for estimating the divergence.

This paper has presented a variety of tests and applications of the hypothesis that smoothed ice drift during the melt season in the central Arctic is described by the free-drift momentum equation (1). Although the intent has been more expositional than conclusive, the results have shown that there is much to be gained from studying ice drift in summer, even if most of the questions regarding mechanical properties of ice are moot.

REFERENCES

Hunkins, K. 1967. Inertial oscillations in Fletcher's Ice Island (T-3). *Journal of Geophysical Research, 72*, 1165–74.

McPhee, M. G. 1975. Ice-ocean momentum transfer for the AIDJEX ice model. *AIDJEX Bulletin, 29*, 93–111.

McPhee, M. G. 1977. A simulation of inertial oscillations in the drift of manned ice stations. *AIDJEX Bulletin, 36*, 65–85.

McPhee, M. G., and J. D. Smith. 1976. Measurements of the turbulent boundary layer under pack ice. *Journal of Physical Oceanography, 6*, 696–711.

Newton, J. L. 1973. The Canada Basin: mean circulation and intermediate-scale flow features. Ph.D. dissertation, 158 pp., University of Washington, Seattle.

Petrichenko, A. N. 1940. Preliminary data on the drift of the *Sedov* for the years 1937 and 1938. *Problemy Arktiki, 2*, 60–85. Transl. for AFCRL, 1953.

Thorndike, A. S., and J. Y. Cheung. 1977. AIDJEX measurements of sea ice motion, 11 April 1975 to 14 May 1976. *AIDJEX Bulletin, 35*, 1–149.